Impact Probability Maps Computation and Risk Analysis for 3D Ground Infrastructures due to UAV Operations

Baptiste Levasseur, Sylvain Bertrand

Impact Probability Maps Computation and Risk Analysis for 3D Ground Infrastructures due to UAV Operations

B. Levasseur[1], S. Bertrand[1]

Abstract— **This paper proposes a methodology for computing the probability of impact on 3D infrastructures (eg. buildings) in the event of an Unmanned Aerial Vehicle (UAV) failure during a flight. This information is essential in risk analysis, whether for the preparation of a mission or for the definition of safety rules by regulatory authorities. Generation of impact probability maps on the infrastructures is based on Monte Carlo simulations involving a dynamic model of a fixed-wing UAV. Two cases are considered to represent different types of structures. The first corresponds to the presence of an infinite vertical plane, a textbook case allowing thresholds to be set conservatively. The second corresponds to a box placed on the ground that can generically encompass many types of infrastructures at risk. Generated probability maps of impact on the infrastructures are given and analyzed for these two cases. The evaluation of the kinetic energy of impact, a fundamental element in the evaluation of damage to buildings, is also addressed.**

I. INTRODUCTION

The use of Unmanned Aerial Vehicles (UAVs) has been growing very strongly in the civil sector for several years. This growth meets a more and more obvious need for many applications in terms of data capture or surveillance, whether for commercial, research or security purposes.

The choice of UAVs is particularly relevant in the context of Long Range Operation missions, especially for the surveillance and maintenance of power lines or railway networks, which implies to operates the UAV beyond visual line-of-sight (BVLOS) [1][2][3]. In this case, fixed-wing UAVs remain the preferred solution due to the considered distances. However, these facilities are generally located close to populated areas or critical infrastructure, which makes it necessary to assess the risk associated with the missions. This risk analysis, which is mandatory to obtain flight authorizations from regulatory authorities, is also important to enable operators to adapt trajectories to guarantee a certain level of safety.

While many methods borrowed from civil aviation [4] attempt to characterize the risk at a global level, it is important to emphasize the need for precise methods that take into account the specificity of the mission as well as the characteristics of the UAV. This is the aim of some methods such as SORA (Specific Operation Risk Assessment) which offer a guideline for risk assessment of UAVs. More quantitative methods such as Probabilistic Risk Assessment (PRA) can also be considered to obtain a precise quantification of the risk. A comparison with SORA can be found in [5]. In PRA, the evaluation of a risk criterion is based on a chain of conditional factors represented by probability laws [1]. These include the probability of failure of the UAV, the probability of impact at ground, the probability of collision with third-parties, depending on the population density or the location of facilities, etc.

Most of the current works in the literature focus on PRA regarding ground impacts and collision with people. Generation of 2D impact footprints [7], [8], [9] or 2D probability maps [10][2] on ground have been proposed. In these works, descent trajectories of UAVs are generated based on different modeling assumptions, eg. ballistic descent [6], 2D kinematic descents while neglecting dynamics [1], reduced dynamic models [7]. In all these works and related ones from the literature, impacts and risks are only evaluated at ground. Some improvements have been proposed to account for the presence of buildings for example, by considering sheltering factors as corrective terms of the computed risks [11]. However, the presence of 3D obstacles such as buildings or infrastructures across the descent trajectory of the UAV has not yet been the topic of in-depth studies, although it can greatly modify the risks induced at ground for people (eg. in urban or semi-urban scenarios). In addition, in the aforementioned works, risks are always considered with respect to people, although some infrastructures may be directly subject to high criticality (eg. buildings, power plants, etc.).

This paper aims at proposing a methodology to account for the presence of 3D infrastructures in risk assessment. Obtained results are of interest both for risks assessment at ground (sheltering factor) and on the infrastructure itself (impacts on critical structures). As a first step, two categories of structures are considered in this paper: a vertical plane and a rectangular box. The first case represents a textbook case allowing a good understanding of the trajectories and thus the definition of conservative thresholds for risk assessment and mitigation. The second case allows a more accurate modeling of numerous infrastructures (buildings, plants, linear infrastructures, etc.).

The proposed approach enables to generate density maps of the probability of impact on these surfaces, as well as the kinetic energy of impact. It is a fundamental asset for operators in operations planning to identify safety margins to guarantee the security of infrastructures, or for regulatory authorities to determine more accurately exclusion perimeters (no fly zones) around critical infrastructures. It should also be noted that the evaluation of the kinetic energy of impact is directly correlated to the damage suffered by the structures [16] and

[1]All authors are with Université Paris-Saclay, ONERA, Information Processing and Systems, 91123, Palaiseau, France. {baptiste.levasseur, sylvain.bertrand}@onera.fr

is therefore of a huge importance in the protection and design of the infrastructure itself.

In this paper, generation of impact probability maps on infrastructure surfaces is based on previous work carried out by the authors [12], where efficient methods for generating 2D impact probability maps at ground as a function of several parameters (wind, altitude and UAV speed) were developed to allow their off-line or on-line uses in the risk assessment process [13]. These impact probability maps were estimated from Monte Carlo simulations on sampled trajectories from a complete 6DoF fixed-wing UAV model. The precise study of the system dynamics also made it possible to analyze the repercussions in terms of kinetic energy at impact.

This paper is organized as follows. First, the methodology of stochastic generation of impact trajectories is recalled, followed by the method of intersection with geometric structures in Section III. The analysis of the school case of impacts in the presence of a vertical plane is studied in Section IV and the more practical case of a rectangular box is addressed in Section V. Finally, conclusions are presented at the end of the paper.

II. Generation of impact probability maps

First, it is worth briefly recalling the impact trajectory generation process developed by the authors in [12], that is used as a basis in this paper. The UAV failure considered is a total power loss, causing engine failure and actuators lock-up at t_0, resulting in a total loss of control of the vehicle and leading to an uncontrolled descent to the ground until impact at t_f. To model this behaviour, a complete 6DoF dynamic model was developed, including full flight mechanics and hence the possibility to take into account accurate effect of environmental parameters such as wind. The control input vector $u = \begin{bmatrix}\delta_a & \delta_e & \delta_r & \delta_T\end{bmatrix}^\top$ is composed of ailerons, elevators, rudder deflections, and thrust command. The state of the dynamical system to be simulated is defined as $\chi = \begin{bmatrix}X^\top & V^\top & \eta^\top & \Omega^\top\end{bmatrix}^\top$ where X is the position vector defined in a local NED frame, V and Ω are the translation and angular velocity vectors in the aircraft body-frame, and η is the vector of Euler angles (roll-pitch-yaw) describing the attitude of the UAV. The wind velocity vector is denoted V_w and is assumed to be represented in the horizontal plane by two parameters V_w, θ_w which correspond respectively to the amplitude (speed) of the wind and its direction (angle). The dynamic model of the UAV can be summarized with the following state-space representation.

$$\dot{\chi} = F(\chi, u, V_w) \tag{1}$$

The ground descent simulation is then obtained by choosing an initial state vector χ_0 as well as the control vector associated with zero thrust, $u_0 = \begin{bmatrix}\delta_{e_0} & \delta_{a_0} & \delta_{r_0} & \delta_{T_0} = 0\end{bmatrix}$ at a time t_0. To compute the resulting impact point at ground, equation (1) is then numerically integrated until reaching a zero altitude.

During a steady flight (in turn or cruise), the space accessible by the state vector and the control input vector is considerably reduced. In order to identify realistic initial conditions χ_0, u_0, it is necessary to represent these in a more intuitive reduced space. A simple way to represent a trajectory for the fixed-wing UAV is to consider two parameters:

- the turn rate $R = d\psi/dt$, where ψ is the heading angle
- the flight path angle $\gamma = \dot{z}/V_a$, where V_a is the aerodynamic speed of the aircraft.

A trim [14] algorithm is applied to convert the reduced parameters into the initial control and state vector. This algorithm consists in canceling the dynamic part of the state equation (1) by considering kinematic constraints, namely the parameters $(V_a, h_0, R_0, \gamma_0)$. From these parameters, the associated state vectors χ_0 and control vectors u_0 are obtained.

To model the stochastic aspect of the impact trajectories, experimental data were gathered on real flights. These data correspond to a cruise-like flight mode in straight line and constant ground altitude. During this flight mode, the data R_0, γ_0 undergoes a divergence from the nominal point $(0, 0)$. This distribution was approximated by a Gaussian distribution in order to sample the values R_0, γ_0. Finally, an uncertainty on the equilibrium position of the actuators was applied in order to model their flapping behavior (the position of the control surfaces remaining constant throughout the glide path). The simulation chain is presented on Figure 1.

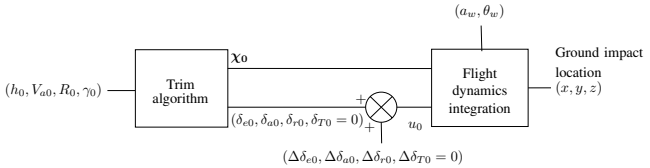

Fig. 1. Simulation flowchart used to generate impact trajectories

It is worth noting the distinction between two types of simulation parameters. On one side the stochastic parameters $(R_0, \gamma_0, \Delta\delta_{e0}, \Delta\delta_{a0}, \Delta\delta_{r0})$ and on the other side the fixed parameters related to a flight condition $(h_0, V_{a_0}, V_w, \theta_w)$.

In order to generate the impact probability maps on the desired plane (ground or surface of the structure), it is necessary to set these external parameters to a given values and to generate Monte Carlo type samples of the stochastic parameters. The trajectories are then simulated until impact. After identifying the impact coordinates, a Kernel Density Estimator [15] is used to estimate the impact probability density function (pdf).

In addition to the probability of impact on a surface, another important piece of information in the risk assessment is the kinetic energy at impact. Several functions directly correlate the kinetic energy at the penetration depth with respect to the material and projectile parameters [16]. In order to be able to use this information in the PRA method, the objective is therefore to obtain maps of kinetic energy at impact. To do this, the 2D sampling of the impact probability maps is replicated and the kinetic energy is mean-averaged in each bin. Note that without the joint reading of the impact pdf, this information can be strongly biased, especially in the case where there is very few impacts in the concerned bin.

III. Impacts on 3D infrastructures

As we are interested in generating impact maps relatively to any possible failure instant during a flight trajectory, a local reference frame used for descent trajectory simulation and impact points computation is defined such that the position coordinates of the UAV at the failure instant t_0 are given by $(x(t_0), y(t_0), z(t_0)) = (0, 0, h_0)$ in this frame and such that the x-axis of this frame is defined along the horizontal component of the velocity vector of the UAV. The instant of impact on ground is denoted t_f and corresponds to $z(t_f) = 0$.
A descent trajectory of the UAV to the ground can then be represented geometrically by the set:

$$\mathcal{T} = \{(x(t), y(t), z(t)) | t \in [t_0, t_f]\} \tag{2}$$

An infrastructure will be defined in a general way by the set of coordinates

$$\mathcal{S} = \left\{(x, y, z) \in \mathbb{R}^3 | g(x, y, z) = 0\right\} \tag{3}$$

where g is the implicit function defining the surface of the structure.
For a given UAV trajectory $\mathcal{T}$, the time of impact t_c on the structure $\mathcal{S}$ is thus given by the first instant of intersection between $\mathcal{T}$ and $\mathcal{S}$:

$$t_c = \min_t \{t \in [t_0, t_f] | (x(t), y(t), z(t)) \in \mathcal{T} \cap \mathcal{S}\} \tag{4}$$

The coordinates of the impact point are denoted $(x_c, y_c, z_c) = (x(t_c), y(t_c), z(t_c)) \in \mathcal{T} \cap \mathcal{S}$.
Note that since the simulated trajectory is sampled in a discrete way due to numerical integration, it is necessary to detect the crossing of the surface and to interpolate the latter in order to have the precise position of the impact point.
Given the computational load required to generate all the impact trajectories for the Monte Carlo simulation process described in the previous section, it is judicious to find a method that limits the number of these simulations. It is interesting to note that, for a given flight mode where the UAV starts from a given initial altitude h_0 with a trajectory $\mathcal{T}$ defined by (2), all impacts related to any structure $\mathcal{S}$ are contained in $\mathcal{T}$. Therefore, the simulation of trajectories can be done first and independently from any structure definition, and by considering a maximum possible value h_{max} for the initial altitude h_0. Computation of impact points can then be done in a second step, using the data basis of all generated trajectories, and for any given structure of interest and initial altitude $h_0 \leq h_{max}$.

A. Ground impacts

The ground impact methodology has already been developed in previous work [12]. Once descent trajectories have been simulated starting from the maximum possible altitude h_{max}, impact points are defined as the intersections of the trajectories with a virtual horizontal plane given by

$$\mathcal{P}_0 = \left\{(x, y, z) \in \mathbb{R}^3 | h = 0\right\} \tag{5}$$

where $h = z - (h_{max} - h_0)$ is the fictitious altitude of the UAV and $h_0 \leq h_{max}$ is the initial altitude to be considered for the UAV.

B. Impacts in presence of an infinite vertical plane

The first case of structure considered in this paper is the textbook case of an infinite vertical plane. In this case, impacts may occur either on the vertical plane or on the ground, depending on the descent trajectories and the location of the vertical plane.
The equation of the vertical plane is then given by :

$$\mathcal{P} = \left\{(x, y, z) \in \mathbb{R}^3 | x \cos\Theta + y \sin\Theta - d = 0\right\} \tag{6}$$

where (d, Θ) are the distance and orientation angle parameters introduced in Figure 2.
In this case, for a given descent trajectory $\mathcal{T}$, the impact point corresponds to the first intersection in time between $\mathcal{T}$ and one of the two planes $\mathcal{P}_0$ and $\mathcal{P}$, which corresponds in (3) to $\mathcal{S} = \mathcal{P}_0 \cup \mathcal{P}$.

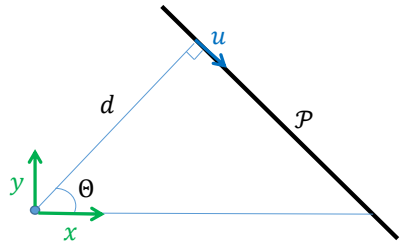

Fig. 2. Geometry of vertical plane with respect to the initial position of the UAV

C. Impacts in presence of a box

The second case of structure considered is a rectangular parallelepiped, or box. In this case, several planes are to be considered, each one being numbered according to the nomenclature introduced in Figure 3. Plane 5 being the "roof" of the box and Plane 0 the ground. The box is characterized by its dimensions (L, l, h_{box}) corresponding respectively to its length, width and height. Its location is characterized by the position of its center C in the plane (x, y) with coordinates (x_b, y_b), and its orientation by the angle Θ (see Figure 3).
Each face is defined by the following set:

$$\mathcal{P}_i = \{(x, y, z) \in \mathbb{R}^3 | g_i(x, y, z) = 0, \\ g_k(x, y, z) \leq 0, k = 0 \ldots 5, k \notin \{i, j_i\}\} \tag{7}$$

for $i = 1, \ldots, 5$, and where j_i is the index of the plane opposite to Plane i in the box (eg. $j_i = 2$ for $i = 1$).
As before, the set defining the box and ground and used for impact computation is then $\mathcal{S} = \mathcal{P}_0 \cup \bigcup_{i=1,\ldots,5} P_i$.

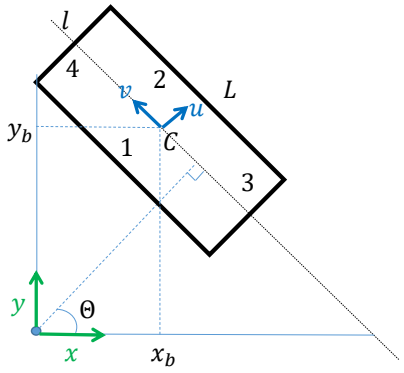

Fig. 3. Geometry of rotated box with respect to the initial position of the UAV

The functions $g_i(x, y, z)$ are defined as follows:

$$
\begin{aligned}
g_1 &= -\left((x - x_b)\cos\Theta + (y - y_b)\sin\Theta - \frac{l}{2}\right) \\
g_2 &= +\left((x - x_b)\cos\Theta + (y - y_b)\sin\Theta + \frac{l}{2}\right) \\
g_3 &= -\left(-(x - x_b)\sin\Theta + (y - y_b)\cos\Theta + \frac{L}{2}\right) \\
g_4 &= +\left(-(x - x_b)\sin\Theta + (y - y_b)\cos\Theta - \frac{L}{2}\right) \\
g_5 &= h - h_{box}
\end{aligned}
\tag{8}
$$

Once the 3D impact points have been selected, they must be projected and centered in the plane in question to get a 2D scattering. The change in variable associated with this transformation is:

$$
\begin{aligned}
u &= (x - x_b)\cos\Theta + (y - y_b)\sin\Theta \\
v &= -(x - x_b)\sin\Theta + (y - y_b)\cos\Theta
\end{aligned}
\tag{9}
$$

IV. Risk analysis on ground without the presence of any infrastructure

Throughout the rest of the paper, the initial position of the UAV will be represented on figures by a red dot at the coordinates $(0, 0)$ in the (x, y) plane. Its initial velocity will be directed along the x axis towards the $x > 0$. All results presented in the rest of this paper correspond to a zero wind with an initial altitude and speed of the UAV respectively set to $h_0 = 150m$ and $V_{a_0} = 20m/s$. Influence of different parameters such as altitude and wind on the probability of impact on ground in the absence of any obstacles has already been studied in depth in previous work carried out by the authors [12].

The probability map of ground impact in the considered study case (no structures) is represented on Figure 4 and will serve as a reference for comparison with the cases with structures.

It should be emphasized that that the probability of ground impact in the region directly in front of the UAV is almost zero. This behavior can be explained by the fact that since the UAV's speed is low, even small variations from the point of equilibrium end up generating a high degree of instability in terms of trajectories. On the other hand, the results show that all trajectories end up converging towards helical descents joining two distinct modes located at $x = 100m$ and $y = \pm 100m$.

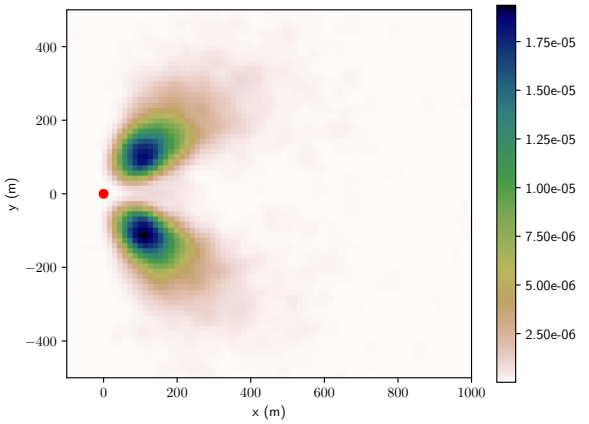

Fig. 4. Probability of impact on the ground without obstacles

The analysis of the mean ground kinetic energy map shown in Figure 5 shows a certain homogeneity in the two modes where the probability of ground impact is high. However, the region of the ground where the kinetic energy at impact is the highest corresponds to the zone directly in front of the initial position of the UAV. This is because the trajectories to this area correspond to very unstable trajectories (very high actuator noise and high fliht path angle) that cause rapid nose-down descent to the ground. It should be noted that given the rarity of these trajectories (near-zero probability of impact), the average kinetic energy in these areas tends to be overestimated compared to areas with a high probability of impact.

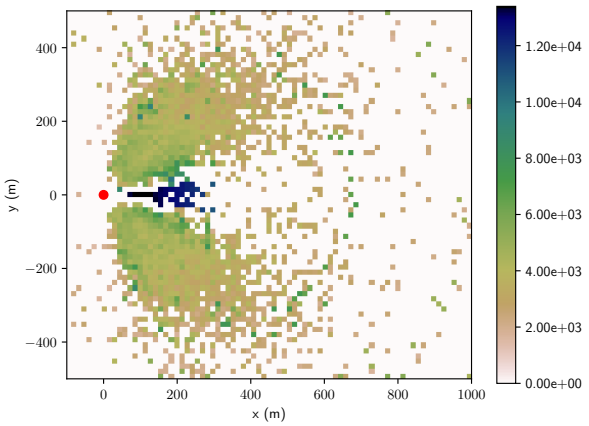

Fig. 5. Kinetic energy of impact on the ground without obstacles (J)

V. Risk analysis in the presence of an infinite vertical plane

Two theoretical cases with an infinite vertical plane will be considered in this section: a first case with a plane orthogonal to the UAV's initial path, i.e. aligned with the y-axis, and a second case with a plane parallel to the UAV's initial path, i.e. aligned along the x-axis. These two theoretical case provide a good understanding of the evolution of the trajectories and their distribution.

A. Plane along y axis

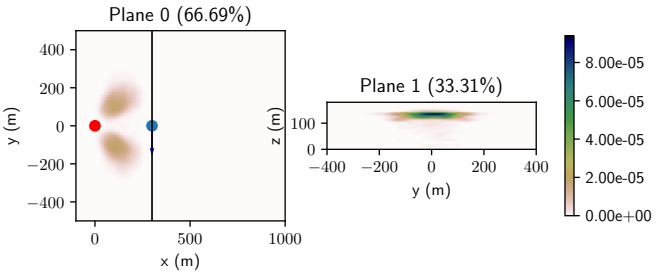

(a)

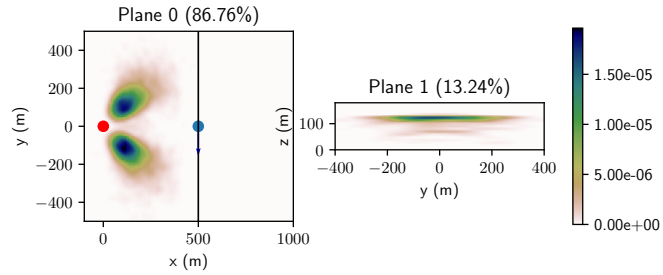

(b)

Fig. 6. Impact probability on each plane with vertical plane along y-axis: (a) $d = 300$m; (b) $d = 500m$

The results for a plane along y-axis located at a distance $d = 300$m or $d = 500$m from the initial position of the UAV are shown in Figure 6. Probability maps are given on ground (Plane 0) and on the vertical plane (Plane 1). The percentages in the plot titles correspond to the ratio of the number of impacts located on the considered plane with respect to the total number of impacts. It can be seen that by placing the plane beyond the two main impact modes ($d > 100$m), the ground impact map remains almost unchanged.The probability of impact on the vertical plane highlights the stratified aspect of the trajectories. Indeed, the only trajectories impacting the vertical plane correspond to those undergoing a very small variation in terms of stochastic parameters. Thus, they correspond to the trajectories in almost rectilinear glide (before the instability makes them enter the helical descent mode towards one of the two ground modes). As a result, there is only a little variation in terms of altitude of the vertical impacts and a large scattering along the y axis that increases with the distance from the plane.

The study of the kinetic energy at impact, for the same

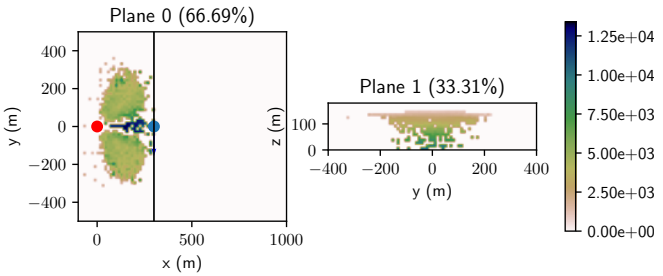

(a)

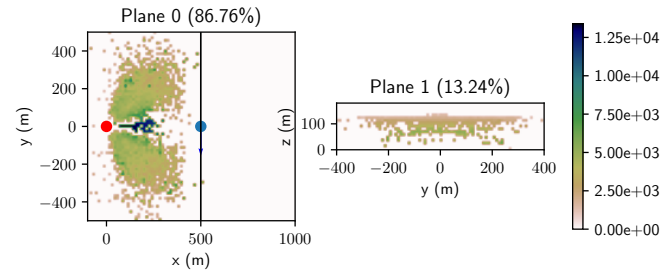

(b)

Fig. 7. Smoothed kinetic energy (in J) on each plane with vertical plane along y-axis: (a) $d = 300$m; (b) $d = 500m$

two configurations, represented on Figure 7, reveals a strong difference between areas with high energy and those with a high probability of impact. Thus, it can be seen that the zone with highest energy is the one directly in front of the UAV (which intersects the plane when it is placed at $d = 150m$). This zone corresponds to nose-down descents reaching very high speeds. However, the comparison with the impact probability map shows that these trajectories remain very rare compared to helical descents, which are stable in terms of kinetic energy. Nevertheless, it can be seen that the kinetic energy on the vertical plane for quasi-rectilinear trajectories (areas of high impact probability) remains lower than the impact energy on the ground. This means that the UAV increases speed during descent. There is therefore a direct correlation between trajectory instability and impact kinetic energy.

To fully understand the influence of the location of the vertical plane, a sensitivity study has been performed on the distance d to the plane. Thus, Figure 8 shows the evolution of the ratio of impacts located on the vertical plane as a function of the distance d to the plane. The maximum probability of impact obtained on each plane is also shown (in logarithmic scale). These graphs can be used, eg. by operators, to set a safety threshold on the distance to be respected.

Another information of interest is the spatial distribution of the impacts on the vertical plane which is shown in Figure 9. The (y, z)-coordinates of the mean position of impact points are represented by the solid lines and the confidence intervals at 1σ are represented by the shaded areas. These

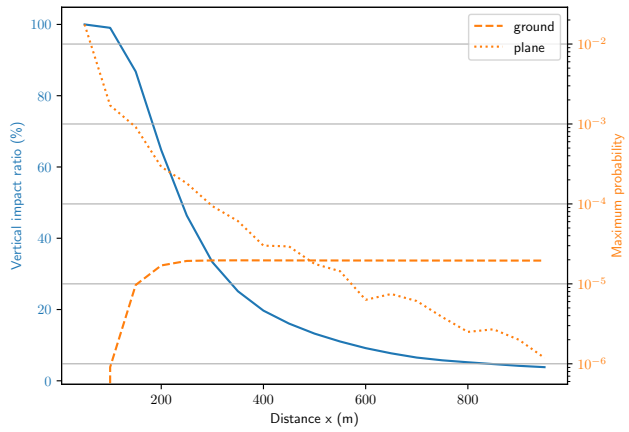

Fig. 8. Ratio of impacts on the vertical plane along the y-axis and maximum probability on each plane.

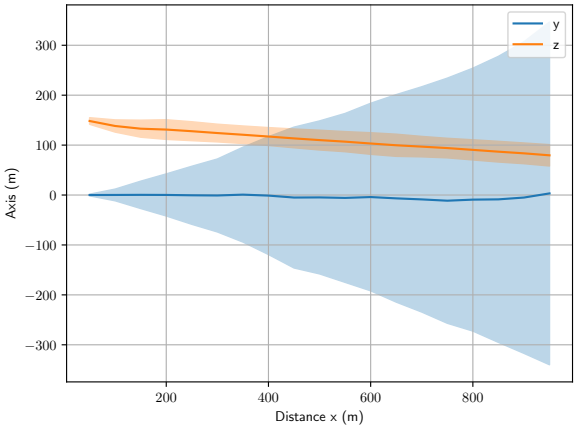

Fig. 9. Coordinates (y, z) of the mean position of impacts on plane and confidence intervals at 1σ for a plane along y-axis

results highlight the narrow distribution of impact altitudes which decrease linearly with the distance to the plane, corresponding to straight glides. On the other hand, if the mean position of the impacts on the y-axis remains centered, its standard deviation grows exponentially, highlighting the increasing instability of the trajectories with distance.

Finally, the evolution of the kinetic energy for each plane is represented on Figure 10. It can be seen that when the plane is too close to the initial position of the UAV, all the impacts take place on the plane and have a low speed. As the plane moves away, it is first the nose-down trajectories that hit the ground, which explains the high mean kinetic energy on the ground. By moving the plane away further, the kinetic energy of impact on both planes converges.

B. Plane along x-axis

The same study is performed for infinite vertical plane colinear to the x-axis but shifted along the y-axis. The plane is placed successively at a distance $d = 150m$ and $d = 300m$

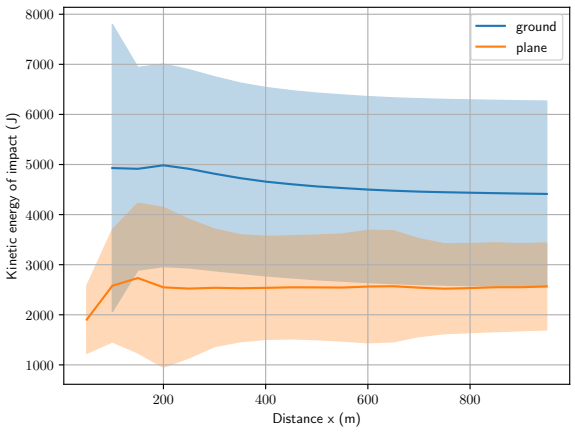

Fig. 10. Mean kinetic energy and confidence interval at 1σ on each plane for a plane along y-axis

from the initial position of the UAV.

The ground and vertical plane impact probability maps are

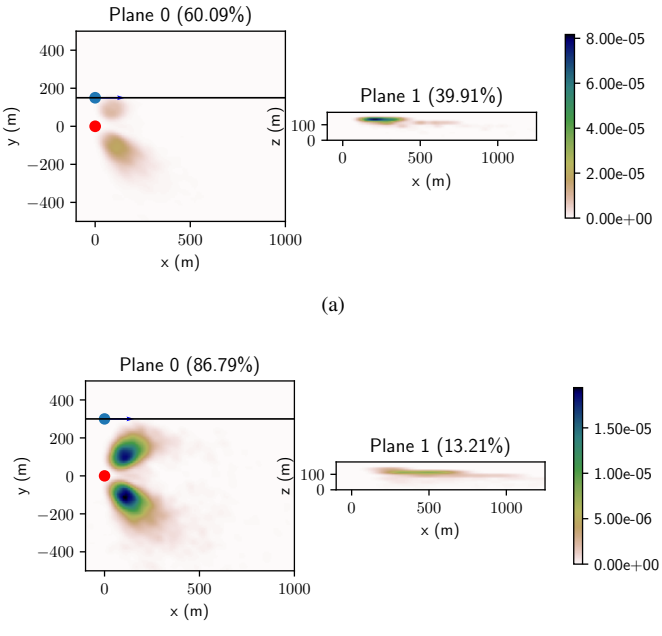

Fig. 11. Impact probability on each plane with vertical plane along x-axis: (a) $d = 150$m; (b) $d = 300m$

shown in Figure 6. Particular attention will be paid to the change in scale from the baseline impact probability map 4. The results in terms of ground impact clearly show the independence of the two probability modes. Regarding the impacts on the vertical plane, the scattering of impacts at a given altitude varies linearly with respect to the x-axis, as shown in Figure 14.

Concerning the smoothed kinetic energy maps shown in Figure 12, complementarity can still be found between the zones of high probability and the zones of high kinetic energy, in particular at the level of impacts at low altitude

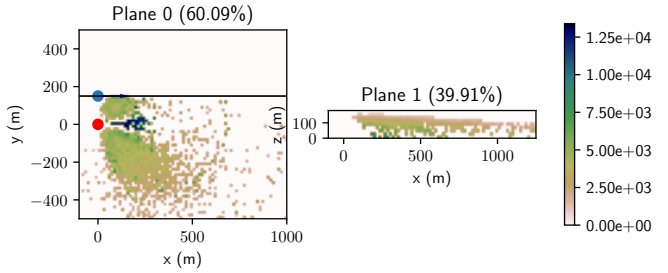

(a)

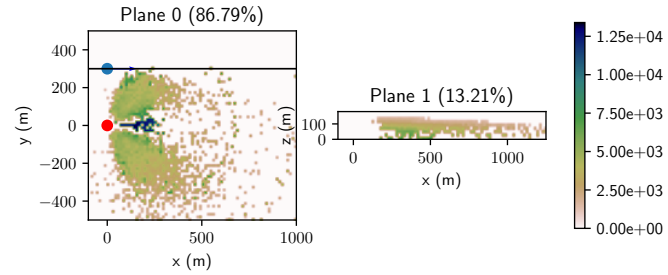

(b)

Fig. 12. Smoothed kinetic energy (in J) on each plane with vertical plane along x-axis: (a) $d = 150$m; (b) $d = 300m$

on the vertical plane which correspond to rapid nose-down descents.

The sensitivity study with respect to the distance d to the plane shows the same trends in terms of ratio and maximum probability as for the vertical plane aligned to the y-axis, as shown in Figure 13. Note, however, that the maximum impact probability for the plane along the y-axis remains two orders of magnitude lower than in the case where the plane is aligned to the x-axis. This result can be explained by the fact that the trajectories start along the x-axis and therefore have time to spread out before hitting the plane. Finally, the fact that the maximum ground impact probability remains constant as a function of the distance from the plane shows the independence of the two ground impact modes.

Finally, by plotting the (x, z)-coordinates of the mean position of impact points on the vertical plane, one can see the linear trend of mean altitude with respect to the distance d to the plane. By considering the position of the impacts on the x-axis, it is interesting to observe that the impact zone moves away as the d distance increases. Thus, it is important to note the existence of a "safe" zone on the structure (i.e. a zone with very few impacts) around the projected position of the UAV on the plane. For example, for distances to the plane of 500m or more, the impact zone on the plane will be located at least 400m away in front of the UAV.

The theoretical study of impacts in the presence of a vertical plane thus allowed the identification of the behaviors of descent trajectories, highlighting altitude layers strongly correlated with distance to the plane. These layers correspond

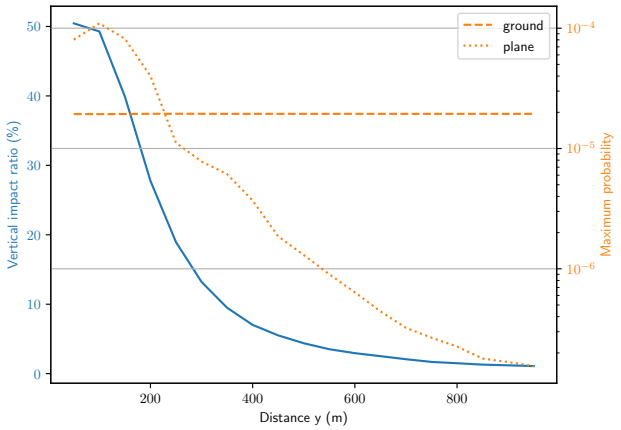

Fig. 13. Ratio of impacts on the vertical plane along the x-axis and maximum probability on each plane

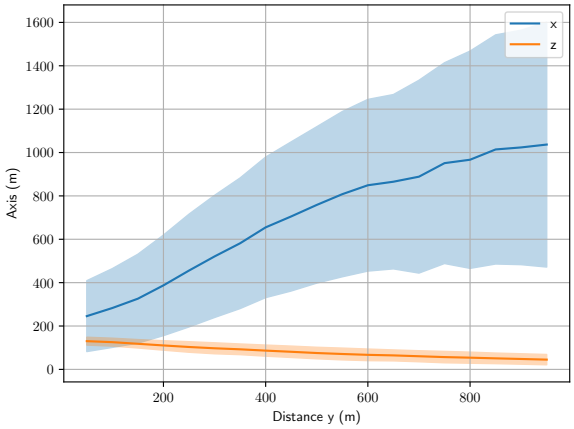

Fig. 14. Coordinates (x, z) of the mean position of impacts on plane and confidence intervals at 1σ for a plane along x-axis

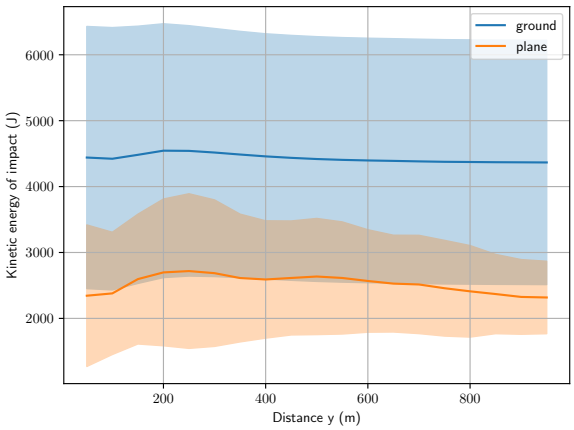

Fig. 15. Mean kinetic energy and confidence interval at 1σ on each plane for a plane along x-axis

to gliding flights with constant flight path angle. The analysis of the evolution of the distribution of impacts both on the ground and on the vertical plane also makes it possible to define safety thresholds in terms of distance in order to guarantee a certain proportion of impact on the plane. These thresholds can be specified using the distribution of impacts on the plane as well as the mean impact kinetic energy.

VI. Risk analysis in the presence of a box

If the infrastructure or obstacle is located in a reduced and bounded area of the flight space, representation by an infinite plane can lead to non accurate evaluations of the risk by being too strict on the exclusion zones. In addition, some phenomena may not be taken into account by an infinite structure representation such as the possibility of circumventing paths around the structure leading to impacts on its opposite side wrt to the UAV initial position.

To represent a structure with finite dimensions, one can use the 3D box previously presented. The dimensions of the box in this study have been chosen so that they include the boundary dimensions of an infrastructure at risk (such as a power plant): $(l, L, h_{box}) = (200, 100, 115)$m. The main axis of the box is considered to be aligned with the initial trajectory of the UAV ($\Theta = 0$). The degrees of freedom studied in this part are the coordinates (x_b, y_b) of the center of the box.

Figure 16 shows the probability maps associated to each

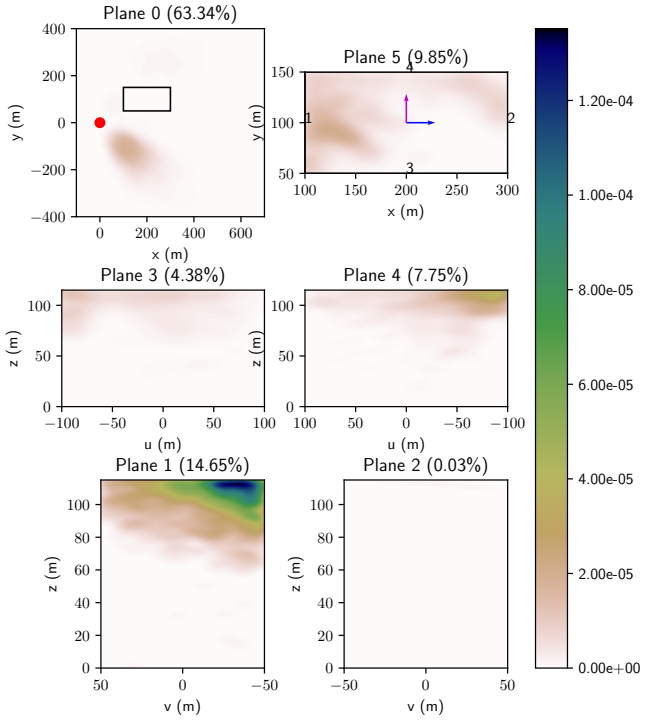

Fig. 16. Impact probability maps on each plane with a box located at $(x_b, y_b) = (200, 100)$m

plane in the case of a box placed in $(x_b, y_b) = (200, 100)m$. This case is particularly critical since the structure is located directly on one of the two main ground impact modes, highlighting a strong interaction of the object with the impact trajectories. Remember that the indices associated to each plane are the ones introduced in Figure 3. For the representation of the maps, a local frame with two axis u and v are introduced, defined in (9). They are respectively plotted in magenta and in blue in the top-right plot of Figure 16. The origin of this local frame corresponds to the center of the box and its axes are aligned with the main directions of the box corresponding respectively to its width and length. It is also worth noticing that the maps are represented on each face as if looking at the face from the outside of the box. (Thus, the axes of planes 3 and 4 are reversed, as are the axes of planes 1 and 2).

As it was shown during the analysis in the presence of a vertical plane, it can be seen that the box only influences the left lateral mode ($y > 0$) at the level of ground impacts. It can then be seen that 36.66% of the impacts take place on the structure. A large part of these impacts then occur directly on Plane 1 located in front of the initial trajectory of the UAV (14.65%), in accordance with the vertical plane study along the y-axis. In addition, it is clear that all the impacts on the structure take place at high altitude, as shown by the analyses in terms of average impact position on the axes of the planes (see Figures 9 and 14). The second face receiving the most impact is the roof of the structure, with nearly 9.85% of the impacts. It is important to highlight the difference in scale between the impacts on the plane directly opposite (1) and the other planes, where the maximum probability varies by a factor of 10. These results also highlight the specificity of the trajectories in the sense that all sides of the box are exposed. Thus, even face 4, which is opposite to the position of the UAV with respect to the structure, receives a high proportion of localized impacts, thus leading to high probabilities of impact.

If one now focus on the kinetic energy of impact on each plane, one can see that the latter is quite low on the structure compared to the impacts on the ground. This is due in particular to the fact that the box is very close to the UAV's initial position and that the trajectories do not have time to gain speed before hitting the box.

Given the complexity of the distributions of impacts on each side and their dependence on the position of the box, a sensitivity study has been be conducted with respect to both x_b and y_b positions of the box. By considering only the ratios of impacts located on the box, it is possible to define a risk map for the structure as a function of the position of the box, as shown in Figure 18. It can be seen that the case study shown in Figure 16 represents one of the worst cases in terms of ratio of impacts on the box. This representation is very useful to define exclusion thresholds (size of no-fly zones) in order to avoid possible structural collisions. However, it does not show the risks incurred by each face of the box.

In order to identify the sensitivity of each face of the box according to its position, the impact ratios for each plane are represented on the figure 19. A complementarity between

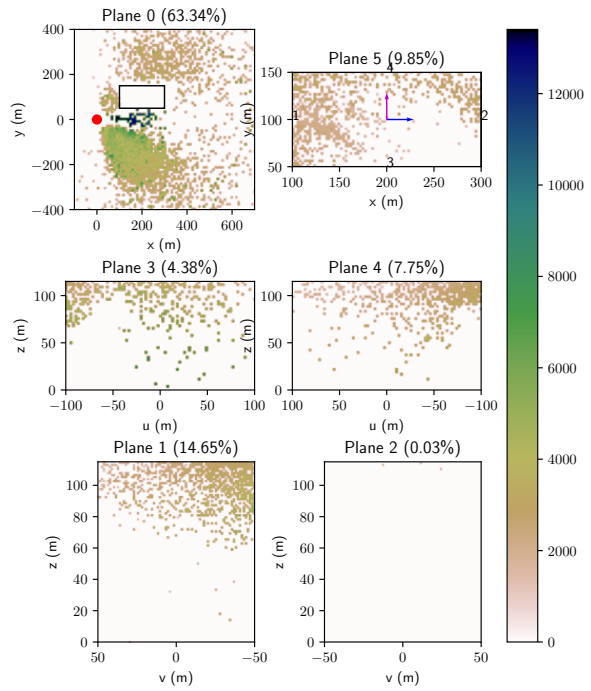

Fig. 17. Smoothed kinetic energy (in J) on each plane with a box located at $(x_b, y_b) = (200, 100)$m

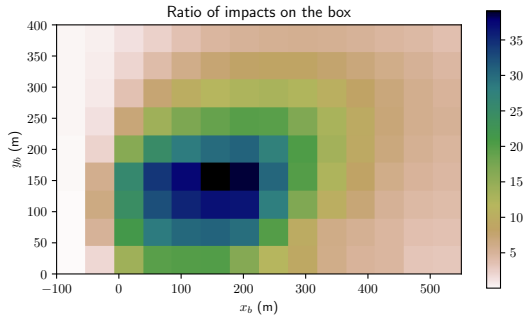

Fig. 18. Ratio of impact on the box w.r.t. the position of the box (%)

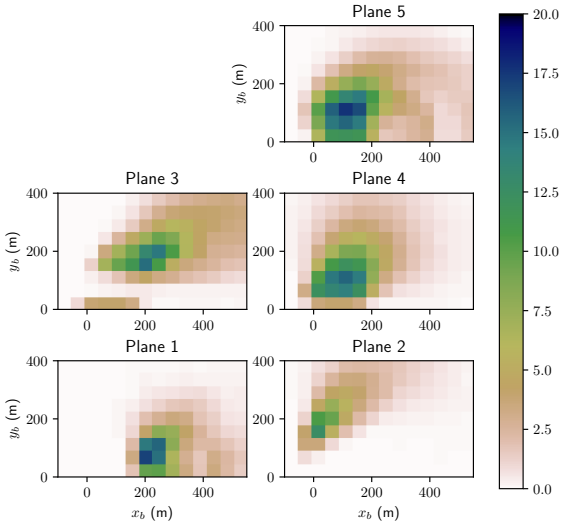

Fig. 19. Ratio of impacts on each plane w.r.t. the position of the box (%)

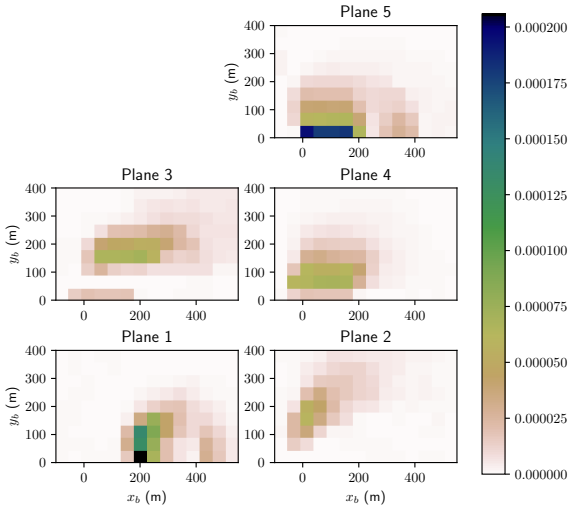

Fig. 20. Maximum probability of impact on each plane w.r.t. the position of the box

some planes can be noticed. For example, when the structure is close to the initial position of the UAV (x_b <200m), the impacts are mainly located on Planes 4 and 5 which represent respectively the opposite plane aligned with the x-axis and the roof. When the structure is further away, it is mainly the front Plane 1 that receives most of the impacts. This representation also shows that the impacts on Planes 2 and 3 (back of the box and plane closest to the UAV aligned with the x-axis) occur when the structure is farther away along the y-axis by a distance y_b >100m.

To quantify the location of collisions with the box, the maximum probability of impact on each plane is represented on Figure 20 as a function on the box location. A strong correlation is observed with the impact ratios on each plane. However, very high probabilities can be distinguished on the roof of the box when x_b <200m and y_b =0m, highlighting key points to be secured.

Finally, average impact kinetic energy maps for each plane are drawn on Figure 21 in order to identify the severity of the impacts and the potential damage they may cause. It is then noted that the box positions with maximum kinetic energy do not necessarily correspond to those with the most impacts. Although this result is smoothed out as the impact ratio increases, critical box positions are observed for certain planes, notably Plane 3 (plane aligned with the x-axis closest to the UAV) for x_b <200m and Plane 1 (from the front) for x_b >200m.

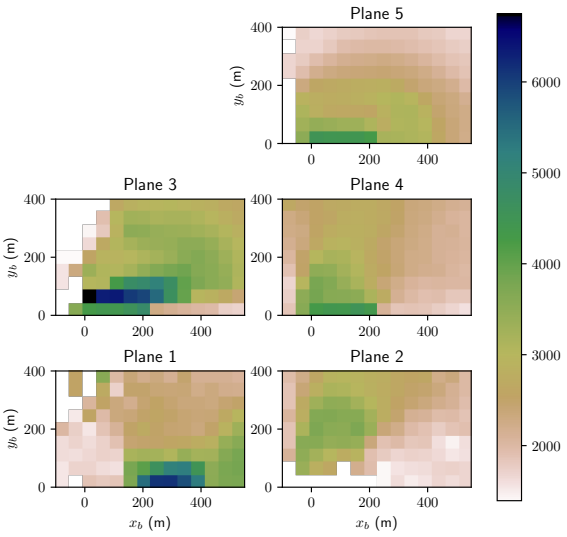

Fig. 21. Mean kinetic energy of impacts on each plane (in J) w.r.t. the position of the box

VII. CONCLUSIONS

The safety of critical infrastructures is a major issue in UAV operations. This criterion can become a key element in the definition of missions, guiding both operators and regulatory authorities. This paper has proposed a method to generate impact probability and kinetic energy maps on a 3D structure located along the trajectory of a fixed-wing UAV. Analysis of the obtained results have be presented for different case studies.

The first more theoretical analysis on infinite vertical planes have provided a good understanding of the behaviour of impact trajectories and thus enabled the development of a methodology for evaluating minimum distance thresholds to be respected. The second study on boxes has emphasized the criticality of certain specific parts of the structures, even when they are opposite to the position of the UAV. Finally, the analysis of the kinetic energy of impact in the two cases has been performed, providing an initial view of the risks of structural damage.

Future work will aim at setting up a global risk definition metric combining both impact probabilities and casualty probabilities for structures. Several reference structures will be studied in order to determine specific exclusion thresholds.

ACKNOWLEDGMENT

This work has been supported by French DGAC in the context of the research partnership PHYDIAS with ONERA for safety improvement of UAVs.

REFERENCES

[1] S. Bertrand, N. Raballand, F. Viguier and F. Muller, “Ground Risk Assessment of Long-Range Inspection Missions of Railways by UAVs”, *International Conference on Unmanned Aicraft Systems*, 2017.

[2] A. La Cour-Harbo, ”Quantifying Risk of Ground Impact Fatalities of Power Line Inspection BVLOS Flight with Small Unmanned Aircraft”, *International Conference on Unmanned Aircraft Systems*, 2017.

[3] S. Bertrand, N. Raballand, F. Viguier, ”Evaluating Ground Risk for Road Networks Induced by UAV Operations”, *International Conference on Unmanned Aicraft Systems*, 2018.

[4] A. Washington, R.A. Clothier, J. Silva, ”A Review of Unmanned Aircraft System Ground Risk Models”, *Progress in Aerospace Sciences*, vol.95, pp.24-44, 2017.

[5] A. la Cour-Harbo, , ”The value of step-by-step risk assessment for unmanned aircraft”, *International Conference on Unmanned Aircraft Systems*, 2018.

[6] A. La Cour-Harbo, “Ground Impact Probability Distribution for Small Unmanned Aircraft in Ballistic Descent”, *International Conference on Unmanned Aircraft Systems*, 2020.

[7] A. Poissant, L. Castana, H. Xu, ”Ground Impact and Hazard Mitigation for Safer UAV Flight Response”, *International Conference on Unmanned Aircraft Systems*, 2018.

[8] P. Wu, R. Clothier, ”The development of ground impact models for the analysis of the risks associated with Unmanned Aircraft Operations over inhabited areas”, *International Probabilistic Safety Assessment and Management Conference and the 2012 Annual European Safety and Reliability Conference*, 2012.

[9] Y. Haartsen, R. Aalmoes, Y.S. Cheung, ”Simulation of Unmanned Aerial Vehicles in the Determination of Accident Locations” *International Conference on Unmanned Aircraft Systems*, 2016.

[10] E. Rudnick-Cohen, J. W. Herrmann, S. Azarm, ”Modeling Unmanned Aerial System (UAS) Risks via Monte Carlo Simulation”, *International Conference on Unmanned Aircraft Systems*, 2019.

[11] S. Primatesta, L. S. Cuomo, G. Guglieri, A. Rizzo, ”An Innovative Algorithm to Estimate Risk Optimum Path for Unmanned Aerial Vehicles in Urban Environments”, *Transportation Research Procedia*, vol.35, pp.44-53, 2018.

[12] B. Levasseur, S. Bertrand, N. Raballand, F. Viguier, and G. Goussu, ”Accurate Ground Impact Footprints and Probabilistic Maps for Risk Analysis of UAV Missions”, *IEEE Aerospace Conference*, 2019.

[13] B. Levasseur, S. Bertrand, N. Raballand, ”Efficient Generation of Ground Impact Probability Maps by Neural Networks for Risk Analysis of UAV Missions”, *International Conference on Unmanned Aircraft Systems*, 2020.

[14] A. De Marco, E.L. Duke and J.S. Berndt, “A General Solution to the Aircraft Trim Problem”, *AIAA Modelling and Simulation Technologies Conference and Exhibit*, 2007.

[15] M.P. Wand, M.C. Jones, ”Kernel smoothing”, *Monographs on Statistics And Applied Probability*, 1995.

[16] R.P. Kennedy, ”A Review of Procedures for the Analysis and Design of Concrete Structures to Resist Missile Impact Effects”, *Nuclear Engineering and Design*, vol.37, no.2, pp.183-203, 1976.